April 21, 2000

Effects of neutral particles on edge dynamics in Alcator C-Mod plasmas.

R. L. Boivin, J. A. Goetz, A. E. Hubbard, J. W. Hughes,
I. H. Hutchinson, J. H. Irby, B. LaBombard, E. S. Marmar,
D. Mossessian, C. S. Pitcher, J. L. Terry,
Plasma Science and Fusion Center
Massachusetts Institute of Technology, Cambridge, MA 02139
B. A. Carreras, L. W. Owen,
Oak Ridge National Laboratory, Oak Ridge, Tennessee, 37831

Neutral particle densities and energy losses have been measured in the Alcator C-Mod tokamak [Hutchinson *et al.*, Phys. Plasmas **1**, 1511 (1994)]. Their effect on the formation and evolution of the edge barrier which accompanies the enhanced confinement regime are discussed. The neutrals can enter the edge dynamics through the particle, momentum and energy balance. Neutral densities of up to $5\text{x}10^{16}$ m^{-3} have been measured in the edge barrier region. Neutrals enter the local dynamics around most of the periphery, not just at the X-point. High resolution measurements of the ionization profile have been obtained for the region near the separatrix. The profile shifts inside the separatrix as the plasma is making a transition from Low to High-mode confinement regimes, partly accounting for the dramatic rise in edge density. The measured neutral density is large enough to affect the bulk ion momentum by charge-exchange, and thereby introducing a negative radial electric field at the edge. At the same time, significant edge heat flux, carried by the neutrals, contributes to the measured power loss. At very high edge densities, this loss mechanism could contribute to quenching H-modes.

I. Introduction

Neutral particles originating from outside the plasma, both from the main chamber and the divertor, have been long believed to affect the dynamics of the H-mode edge barrier. However, standard scalings for local and global thresholds do not involve neutral particles directly, and consequently, neutrals are usually referred to as a hidden variable.[1] For example, previous work done on DIII-D[2–4] pointed to effects due to neutrals on fueling, the formation of the density pedestal, particle confinement time, and on the plasma rotation near the edge, in which for example, the neutrals can modify the conditions for an L-H transition. In addition, work done at the Japan Atomic Energy Research Institute's Fusion Torus-2 Modified (JFT-2M[5]), indicated that the presence of neutrals may actually promote the transition to H-mode. However, the analysis has always been hindered by the lack of direct measurement of the neutral density profile inside the separatrix. This analysis is further complicated by the possibility of different density regimes, for which the neutrals can enter the edge dynamics through separate mechanisms.

The charge-exchange mechanism is a phenomenon which characterizes neutral deuterium particle behavior at the edge of tokamak plasmas. The relative predominance of charge-exchange over ionization increases the penetration of neutral deuterium into the high temperature plasma, and increases momentum and heat transfer across field lines. Since the charge-exchange cross-section is large at conditions of interest, the effects of neutrals can be rather large at the edge, even in the presence of a small number of neutrals. Consequently, this mechanism affects the edge dynamics through the particle,

momentum and energy balances. This paper reports direct measurements of neutral density and power loss, which enable us to evaluate quantitatively the importance of neutral effects.

II. Experimental technique

The Alcator C-Mod tokamak is based on a compact design (R_o=0.67 m, a=0.22m, $\kappa \sim 1.6$), operating at high particle and power densities. Discharges discussed in this paper were obtained with a closed divertor in a single-null configuration with the ion ∇B drift direction towards the X-point. Neutral pressures are usually relatively high, reaching $\lesssim$ 1mTorr in the main chamber, and $\sim$ 100mTorr in the divertor. The first wall components are made of molybdenum, and the wall conditioning consists primarily of periodic boronization. Auxiliary heating consists of Ion Cyclotron heating (ICRF) only, and as a consequence, no central fuelling source is present, and no direct momentum is applied to the plasma.

High confinement regimes (H-modes) are readily obtained in Alcator C-Mod, both ohmically and with ICRF. These H-modes mainly fall into two categories. The first type, the (Edge-Localized-Mode) ELM-free H-mode,[6] exhibits the best energy and particle confinement, but eventually reaches a radiative collapse. The second type, referred to as Enhanced D_α H-Mode (EDA),[7] exhibits a good energy confinement (near ELM-free levels) but is accompanied by a lower particle confinement. In the first case, edge pedestals are very narrow, with density pedestal widths as low as 3-4 mm, and the temperature pedestal being 8-10 mm wide. In the EDA case, these widths

are found to increase.

Recently, a series of new diagnostics has been implemented in order to measure the effects of neutral particles on the plasma edge of the main chamber, especially in the H-mode pedestal region. Profiles of deuterium Lyman-α emission are measured with a 20 channel photodiode array. This array views the edge of the plasma tangentially with an approximate 4 cm span near the separatrix, 12.5 cm below the midplane. This location is found to be representative of the average neutral density found inside the separatrix, avoiding the extremes that could skew the interpretation(see Sect: IIIA). Contrary to similar observations made in the divertor region of Alcator C-Mod,[8] recombination and opacity are not encountered in the cases presented in this study. This measurement, combined with edge electron density and temperature, gives the local ionization rate and neutral density, using well-established excitation rates.[9]

The temperature and density are primarily obtained using the edge Thomson scattering system, which views the edge of the plasma at the top of the discharge. It consists of 16 channels, with a nominal radial spacing of 1mm (when mapped to the midplane). Additional information on the electron density is obtained via the visible continuum (bremsstrahlung) emission, measured by an array which views the discharge tangentially, at the midplane with 2048 chords and a 0.5mm radial resolution. Fast scanning Langmuir probes, and a grating polychromator are also used to complement our electron diagnosis on both sides of the separatrix. The heat flux carried by neutrals is measured using two sets of bolometers with the same tangential

view of the plasma near the midplane, with one set normally sensitive to neutral flux, the other not.[10] The neutral pressure is obtained via ionization gauges located at the wall of the tokamak.

The importance of the neutral population near the edge of the plasma has been also explored using a simple Monte-Carlo algorithm. Since the physical dimensions of interest (i.e. pedestal width) are comparable to the neutral particle mean free path, such a particle following code is more appropriate than a fluid model. The code is based on the pseudo-collision algorithm developed by Heifetz,[11] which follows particles, and through collisions, calculate the probabilities of ionization and charge-exchange. Since the mean-free path is on the order of one centimeter, small compared to the circumference of the plasma, we can use a slab model in the radial direction only. In the absence of neutral beam ions, only electron ionization and charge-exchange events are considered. Recombination is also neglected. Neutral particles are launched from the wall at the Franck-Condon energy and followed, until they get ionized or returned to the wall. Input parameters include the density and temperature profiles, and neutral flux from the outer boundary (vacuum side). The grid size is usually chosen to be smaller (typically 0.2mm) than the temperature and density gradient scale-length, which are on the order of a few millimeters or more. Since ion densities and temperatures are not readily available near the edge, they are derived from the electron density and temperature. With the high densities encountered on Alcator C-Mod, we assume that $T_i \sim T_e$ and we take $n_e = n_i Z_{eff}$. With this simple procedure we obtain the following profile information: neutral density, ionization rate,

power flow to ions, power flow to neutrals and Ly_α emission. The simulation results have been compared with fluid-based modeling (i.e. FRANTIC[12]) and good agreement has been found. Comparison with DEGAS2 have been initiated but lack of radial resolution (inside the separatrix), has, so far, limited the detailed quantitative comparison.

III. Edge Dynamics: L and H-mode

A. Particle Balance

The observed Ly_α emission profile, as shown in Fig. 1a, is very peaked near the separatrix, with a radial extent of 1-1.5 cm. This is a L-mode discharge with I_p = 0.8 MA, B_T=5.4 T, P_{RF}= 1.2 MW, $\bar{n_e}$ = 2.1 x $10^{20}m^{-3}$ and p_o = 1.0 mTorr at the midplane. Also shown is the Monte-Carlo neutral transport simulation for the same conditions, which shows good agreement with the observed profile. With the electron density and temperature profiles (shown in Fig. 1d), we infer the ionization rate and neutral density profiles (see Fig. 1b and 1c) by using the standard branching ratio and cross-sections.[9] Also shown is the calculated profile from the same simulation, again with good agreement. In typical L-mode conditions, we observe that the ratio of the total ionization source inside versus outside the separatrix is nearly 1 to 1. This experimental result illustrates the influence of charge-exchange on neutral transport. It shows that the neutrals can reach a region of much higher temperature than their ionization potential, without the charge-exchange process the neutrals would be all be ionized in the scrape-off

layer before reaching the separatrix. For the neutral density profile, we also observe the expected rapid radial decrease at the separatrix, again in good agreement with the simulation. Overall, the uncertainties are dominated by the sensitivity calibration of the detector, and input density and temperature measurements, with very little contribution from the Abel inversion process.

Our neutral density measurements inside the separatrix have also revealed a marked insensitivity to the neutral pressure at the wall. This non-linearity has also been recognized recently by modeling done for DIII-D discharges.[4] Thus, in assessing the influence of neutrals, the wall neutral pressure measurement can lead to wrong conclusions. Shown in Fig. 2 are a) the neutral density, b) the neutral pressure (measured at the wall) as a function of the average electron density, and c) the ratio of neutral density to the local electron density (both measured at 2mm inside the separatrix). It is remarkable that for a range of 100 in neutral pressure the neutral density varies at most by a factor of 5 or so. Also noticeable is that the neutral density inside the separatrix decreases only slightly while going into H-mode. Consequently, the ratio of neutral density to the local electron density does not vary greatly with electron density, a somewhat unexpected result considering the range of neutral pressures and electron densities. The importance of this observation will be further discussed in the next section.

A well-known characteristic of a H-mode is the drop in D_α emission. We observed a similar behavior in Ly_α emission during an ELM-free H-mode, as shown in Fig. 3. However, although the Ly_α emission is decreasing across most of the profile, following a transition from L to H-mode, the ionization

rate actually increases; the ratio of ionization to photon emission actually increases with density.[9] This effect is especially pronounced at densities above 1x10^{20}, which are readily found in the pedestal region. Similar results have been obtained for DIII-D discharges.[3] Finally, although the neutral density does not vary much inside the separatrix, we observed a small steepening of its local gradient.

Since we are presently measuring the neutral density at only one location, we initiated a study of the poloidal distribution of the neutral density using DEGAS2, as shown in Fig. 4. The neutral density calculated at 5mm inside the separatrix, is plotted as a function of the poloidal angle.[14,15] The modeling uses as input the electron temperature and density, both inside and outside the separatrix, as measured by the ECE, Thomson and Langmuir probe systems, in addition to a series of imbedded probes in the divertor. Additional inputs include the Z_{eff}, H_α emissivity across the full cross-section and full magnetic geometry including a non-orthogonal grid, which is especially important near the X-point. The model includes recycling on divertor and wall (including the inner wall, limiters and antennas) surfaces (using molybdenum reflection coefficients), with the best fit obtained while comparing the ion fluxes to the walls, recycling rates and corresponding fueling rates and consequent neutral distribution. Unfortunately, this is the only run available which covers the main chamber plasma appropriately and corresponds to a L-mode discharge obtained before the Lyman alpha diagnostic was installed. The discharge is a ohmic plasma, with I_p = 1.0 MA, B_T=5.4 T, $\bar{n_e}$ = 1.3 x 10^{20}m^{-3} and p_o = 0.03 mTorr at the midplane. Updated simulations are

under way, especially in view of the many new diagnostics now available for the edge of the main plasma. A few striking points emerge from this first simulation result. The neutral density exhibits a relatively broad poloidal extent, not limited to a small portion of the cross-section (such as the X-point). In fact, the peak in neutral density is not at the X-point, but rather follows the surfaces close to the inner wall, and to the protection limiters and antennas on the outer boundary. This is a direct result of the fact that the main chamber fueling is tied to recycling in the main chamber, not from the divertor.[16–18] Also shown on the poloidal distribution, is the location of the Lyman alpha diagnostic. In this case, the location is characteristic of the average neutral density (inside the separatrix), thus avoiding the extremes such as the midplane inner wall, or at the top of the discharge.

Consequently, to a good approximation, by using poloidal and toroidal symmetry, we can calculate the total ionization rate, both inside and outside the separatrix, by integrating over the profile. Shown in Fig. 5 are the total ionization rates as a function of time. We observe a marked increase in the total ionization rate inside the separatrix during the H-mode phase. This increase amounts to 5.0 $\pm$ 1.0x10^{21} ionizations/sec over the L-mode level found at 0.6 sec. Comparatively, at the same time, the change in the total number of particles (dN/dt), was found to be 3.0 $\pm$ 0.5 x10^{21} /sec. Thus, there is a sufficient increase in ionization rate to explain the change in the total number of particles, changes in the ionization source are an important factor in the particle balance. Conversely we observe that in the case of EDA H-modes, the total ionization rate, inside the separatrix, returns to the L-

mode level after a brief ELM-free period. At that time, the density levels off. The discharge remains in a higher particle confinement, but with an L-mode ionization rate level.

Recent theoretical investigation into the formation of the plasma density pedestal has focused on the importance of neutrals. One model, based on the dynamics of edge transport barriers[19] considers the case where the plasma flux would be balanced by ionizing neutral flux, and consequently a transport barrier, i.e. a pedestal, would form. The derivation is simply based on solving the coupled set of differential equations for the neutrals and the electrons (or the ions), in which only ionization is considered, with neutral flux originating from outside the plasma in a slab geometry. We solve for

$$\frac{\partial n_e}{\partial t} + \frac{\partial \Gamma_e}{\partial x} = \langle \sigma v \rangle \, n_e n_o \tag{1}$$

$$\frac{\partial n_o}{\partial t} + \frac{\partial \Gamma_o}{\partial x} = - \langle \sigma v \rangle \, n_e n_o \tag{2}$$

where the fluxes are simply given by:

$$\Gamma_e = -D \frac{\partial n_e}{\partial x} \tag{3}$$

$$\Gamma_o = -V_n n_o \tag{4}$$

By evaluating the steady-state situation, one obtains for the neutral density:

$$n_o(x) = n_o(a) \exp[-\frac{\langle \sigma v \rangle}{V_n} \int_x^a n_e(x) dx] \tag{5}$$

assuming $n_e(a) = 0$, where a is the radius of the base of the pedestal, assumed to be also the location of the separatrix. The electron density is then described by the following differential equation:

$$D\frac{\partial n_e}{\partial x} = V_n n_o(a) \exp[-\frac{\langle \sigma v \rangle}{V_n} \int_x^a n_e(x) dx] \tag{6}$$

By solving the equation for n_e, they obtained the familiar hyperbolic tangent function with width and height given by:

$$W_{ne} = 2\sqrt{\frac{D}{2\nu_i(a)}} \tag{7}$$

$$H_{ne} = n_o(a)\sqrt{\frac{2V_n^2}{D\nu_i(a)}} \tag{8}$$

where D is the usual particle diffusion coefficient, $\nu_i(a) = \langle \sigma v \rangle n_o(a)$ is the ionization frequency evaluated at the base of the pedestal, $V_n(a)$ is the average neutral velocity originating from outside the plasma, and $n_o(a)$ is the neutral density at the base of the pedestal.

Since we measure the neutral density, and consequently the ionization frequency, we evaluated the widths and heights for various discharges obtained on Alcator C-Mod. Since D is the residual diffusion (in the pedestal region), we used the expression for neo-classical diffusion in the Pfirsch-Schlüter regime. In order to evaluate the height, we calculated the incoming neutral flux $n_o(a)V_n(a)$, as simply being the measured total ionization rate inside the separatrix, divided by the area of the separatrix. Shown in Fig. 6 is the calculated width as described by this model versus the measured width of the pedestal using the visible continuum diagnostic. This diagnostic measures the

bremmstrahlung emission from which we can derive the local electron density with a very good time and very good radial resolution through the whole pedestal region. The data compare well with Thomson scattering data for which they are available simultaneously. Also shown is the calculated density pedestal height versus the measured height. These data were obtained from a set of discharges in which the plasma attains quasi steady-state conditions (EDA H-mode) after an L to H transition. At that time, usually 20-50 msec after the transition, the pedestal is fully formed and transients are avoided. Data points include a range of plasma currents, and a density scan at 0.8 MA. The error bars are derived from the uncertainties of the input variables to the model, and are typical for all points shown. In both aspects of the model we obtain a fairly good agreement, in spite of its simplicity and the small number of plasma parameters. In the case of the density pedestal height, we observe a notable factor of 2 with the model. However, a correlation remains and further refinements (model and measurements) are needed in order to conclude definitely. As reported previously,[20] we also recover the trend of smaller widths at high plasma current and vice-versa. Further refinements of the model are underway, especially in considering a non-zero density outside the pedestal.

B. Momentum Balance

It is believed that rotation plays a very important role in the formation of the H-mode barrier, by reducing the effects of turbulence on transport. It has been suggested that the conditions required for entering H-mode con-

finement can be affected by neutrals. The neutrals can remove and transport momentum by charge-exchange across field lines. Evidence of this effect has been gathered on the Texas Experimental Tokamak (TEXT[21]) that neutrals are affecting the rotation found at the edge. In this picture, the neutrals cause additional viscosity which may damp the rotation. Recent work on DIII-D,[4] outlined some dependence of the power threshold on the neutral viscosity and mean free path.

Recently, the neo-classical derivation of ion flow has been revisited by Fülöp *et al*[22] and Krashenninikov *et al*[23] with the presence of neutrals. They found that, in addition to the neo-classical component(V_{neo}) and the possible presence of anomalous flow (V_a), the neutrals introduce 2 new terms in the ion flow:

$$V_{\|i} = V_{neo} + V_n + V_\pi + V_a \tag{9}$$

In this discussion, we are concentrating on the first three terms. The V_n term corresponds to a direct modification of the ion distribution function, through a change in the pressure anisotropy from which parallel flows may result. By following the various terms in the momentum equation, and in which previously neglected neutral terms are now kept, they obtained:

$$V_n = \frac{-0.09B}{Mp_i\langle(\nabla_\| B)^2\rangle}\frac{\partial}{\partial\psi}\left\langle\frac{(\nabla_\| B)\vec{\nabla}\psi\cdot\vec{\nabla}(n_o T_i^2)}{n_i(\langle\sigma v\rangle_{cx}+\langle\sigma v\rangle_{ion})}\right\rangle \tag{10}$$

The V_π term corresponds to the change in the viscosity due to the neutrals, which are calculated from their effects on the ions given by the stress tensor. In this case, the contribution to the ion flow is given by:

$$V_\pi = \frac{0.11B}{\tau_i p_i \langle (\nabla_\parallel B)^2 \rangle} \frac{\partial}{\partial \psi} \left\langle \frac{\vec{\nabla}\psi \cdot \vec{\nabla}[B n_o T_i (V_{\parallel i} + \frac{2q_{\parallel i}}{5p_i})]}{n_i(\langle \sigma v \rangle_{cx} + \langle \sigma v \rangle_{ion})} \right\rangle \tag{11}$$

Since the neutral mean-free path is short, the neutrals are assumed to acquire the local ion temperature and, at a density ratio $n_o/n_i \gtrsim 10^{-4}$, they can dominate the momentum transport.

Also, by first looking at conservation of toroidal momentum, and in the case where the neutral density is large enough so that neutral viscosity is much larger than the ion viscosity the electric potential is then constrained to satisfy[24]:

$$e\frac{\partial \Phi}{\partial \psi} = -\frac{T_i}{p_i}\frac{\partial p_i}{\partial \psi} - \frac{9}{5}\frac{B^2}{\langle B^2 \rangle}\frac{\partial T_i}{\partial \psi} \tag{12}$$

Of course, the electric field derived from Eq. 12 must then be inserted in the perpendicular momentum balance in order to self-consistently determine the perpendicular ($\vec{E}$x$\vec{B}$) ion flow velocity.

Since we are now measuring the neutral density with high radial resolution, along with local density and temperature, we can evaluate the various terms in Eq. 9 and 12. However, since the expression involves second derivatives, we first fitted the data with the usual hyperbolic tangent functions. These fits proved to be very reliable in characterizing the various parameters without losing accuracy. It turns out that the neutral density profile can also be represented by a hyperbolic tangent function, at least near the pedestal itself. Shown in Fig. 7a is $V_{\parallel i}$ as a function of radius for L and H mode time slices taken from an ELM-free H-mode case (shot #990920024, Ip=1.15 MA, $\bar{n}_e$= 2.1x10^{20}). In this particular case, the parallel velocity is

dominated by the neutral terms (V_n and V_π), and the neoclassical component was found to be less than ∼5km/sec across the edge profile. Fig. 7b shows the E_r from Eq. 12, for the L and H-mode cases. In spite of a relatively small neutral density ($n_o/n_e \sim 10^{-4}$), the effects are pronounced. Ion flow can reach tens of km/sec while the electric field can reach -50kV/m or more. Clearly this effect would not be present with ions alone, as shown by the two curves calculated for the H-mode case of Fig. 7b, with and without the neutrals. Presently, no direct measurement of the ion velocity and radial electric field are available and direct comparison are not possible. In addition, the uncertainty of these two quantities, especially the velocity, is rather large and experimental verification of the model is required. However, the derived magnitude of these two variables indicates a significant role, and fall in the same range than other indirect measurements presently available on Alcator C-Mod.[25] Also, since the important variable is n_o/n_e, and not simply the neutral density, this result may not be unique to Alcator C-Mod.

C. Energy Balance

The final consequence of the charge-exchange process concerns the energy balance, again near the edge of the plasma. Since neutrals can penetrate some distance inside the separatrix, they can sample regions of relatively large temperature. Just as they were able to carry momentum across field lines, neutrals can increase heat transport and influence the edge dynamics. The power loss is predominantly from ions, a smaller amount of power is carried away from the electrons for each ionization event.

It has long been recognized that standard (foil) bolometers are sensitive to escaping power flux carried by neutrals. Although they are not impurity-induced power loss through electromagnetic radiation, they represent nonetheless a power loss from the plasma. The difficulty arises though when one needs to specifically account for these losses. Since the plasma is opaque to these neutrals, optically thin inversion algorithms for obtaining total radiated power or local emissivity may not be strictly valid. Recently, we added a new set of detectors[10] which are not sensitive to radiation carried by neutral particles, at least for neutrals of low energy ($\lesssim$ 500 eV), a situation encountered on Alcator C-Mod since no heating neutral beams are present. Both arrays of bolometers, presently 16 channels each, are viewing the plasma tangentially near the midplane, thus giving the local radiated power emissivity as a function of major radius. The difference between the 2 emissivity profiles thus represents simply the power emissivity carried by neutrals.

As one would expect, the observed power emissivity from neutrals (see Fig. 8) is highly localized very near the edge, as shown for an H-mode case. Radial localization is limited by the intrinsic resolution of both systems, nominally with 2cm radial resolution. The uncertainties are derived from the calibration uncertainty of both bolometric systems. In most cases, the neutral power emissivity is comparable in amplitude to the local impurity radiation, but limited to a region of 1-2 cm near the edge. However, since the volume of that shell is larger than one closer to the center, the total power loss is non-negligible although not necessarily dominant. Also shown,

are the results of the neutral transport simulation for the same case, as used in Sect. IIIA. We see a good agreement between the 2 curves. The calculated power loss has been convoluted with the detector radial resolution. Those simulations, show in fact that the bulk of this power loss originates from inside the separatrix, when we do not include the detector radial resolution. We observed that although the neutral population can drop a little or remains constant at the pedestal location, during an H-mode, the large rise in both the local density and temperature mean a net increase in neutral power loss, whereas these two parameters actually dropped outside the separatrix during the H-mode. This would imply that during ELM-free H-modes the neutral power loss would increase together with the plasma density and could contribute in quenching the H-mode. We also observed that these losses are considerably reduced during EDA H-mode, contributing to a good energy confinement.

IV. Conclusions

High resolution measurements of hydrogenic neutral density, ionization rate and power losses have been obtained on Alcator C-Mod. The results suggest that neutrals are an important factor in the formation of the density pedestal found in H-modes. They may actually determine its characteristic through its width and/or height. It has been found also that neutrals are sufficiently dense to affect the ion momentum in the edge and consequently influence the ion flow near the separatrix. Finally, we found that charge-exchange neutrals also contribute to the local heat balance at the

edge. However, this effect does not appear to be the dominant factor, in low and medium density plasmas. Overall, the effects of neutrals operate differently through the particle, momentum and energy balance, varying in relative importance depending on the regime, in which density being one of the big factors. A complete description must include these 3 elements in a consistent manner, in order to fully evaluate their impact on the edge dynamics. Definite conclusion requires a dedicated experiment in which neutral density can be varied independently of the plasma density. However such an experiment is very difficult to design in view of the very strong coupling between the two parameters.

V. Acknowledgments

We thank the Alcator C-Mod engineering and technical crew for their expert operation of the tokamak. We acknowledge very useful and insightful discussions with M. Greenwald, P. Helander and P. Catto. Work supported by Department of Energy cooperative agreement DE-FC02-99ER54512.

Figures

FIG. 1. Measured radial profiles (dotted lines) of the a) deuterium Ly_α emission, b) ionization rate, c) neutral density near the separatrix, d) electron density (line) and temperature (dash line) profiles obtained in L-mode conditions. Also shown are the results of a 1-D Monte-Carlo neutral transport simulation (lines).

FIG. 2. a) Measured neutral density (at 2 mm inside the separatrix), b) midplane neutral pressure (measured at the wall) and c) ratio of neutral density to the local electron density (both measured at 2mm inside the separatrix), as a function of the average electron density.

FIG. 3. Measured radial profiles of the a) Ly_α emissivity, b) ionization rate and c) neutral density, for L-mode (line) and fully established ELM-free H-Mode (dash line) conditions.

FIG. 4. DEGAS2 simulation of the neutral density found 5 mm inside the separatrix, as a function of the poloidal angle, calculated for the L-mode shot #960113031. Also indicated by a star is the poloidal location of the Ly_α view.

FIG. 5. Total ionization rate, inside (smooth line) and outside (dashed line) the separatrix versus time, for a discharge exhibiting L (shaded) and H-mode periods. Also shown is the measured dN/dt for the same discharge.

FIG. 6. a) Comparison of modeled density pedestal widths (y-axis) with widths measured (x-axis) by the visible continuum diagnostic. b) Com-

parison of modeled density pedestal heights (y-axis) with heights measured (x-axis) by the edge Thomson system.

FIG. 7. a) Derived ion parallel velocity profile for L (line) and H-mode (dash line) near the separatrix. b) Derived radial electric field for L (line) and H-mode (dash line) at the edge pedestal location. Also shown, is the electric field derived without neutrals (dot-dash) for the H-mode case. In this case I_p = 1.4 MA, B_T=5.4 T, P_{RF}= 2.0 MW, $\bar{n_e}$ = 1.5 x 10^{20}m^{-3} in the L-mode phase, $\bar{n_e}$ = 2.6 x 10^{20}m^{-3} in the H-mode phase and p_o = 0.24 mTorr at the midplane.

FIG. 8. Measured power emissivity profile for radiation carried by neutrals. The peak in neutral power emissivity lies at the edge. Also shown are the calculated neutral emissivity (dot-dash) using the 1-D Monte-Carlo neutral transport code and the emissivity profile (dash) from electromagnetic radiation (photon) only. In this case I_p = 1.0 MA, B_T=5.4 T, P_{RF}= 1.0 MW, $\bar{n_e}$ = 2.5 x 10^{20}m^{-3} and p_o = 0.25mTorr at the midplane

References

[1]T. Fukuda, *Plasma Phys. Control. Fusion*, **40**, 543 (1998).

[2]M. A. Mahdavi, N. Brooks, D. Buchenauer, et al., *Journal of Nucl. Mat.*, **177**, 32 (1990), Presented at the 8^{th} PSI Conference, Bournemouth, May 1990.

[3]M. E. Rensink, S. L. Allen, A. H. Futch, et al., *Phys. Fluids B***5**, 2165 (1993).

[4]B. Carreras, L. W.Owen, R. Maingi, et al., *Phys. Plasmas*, **5**, 2623 (1998).

[5]Y. Miura, Y. Asahi, K. Hanada, et al., Divertor biasing effects to reduce the L-H power threshold in the JFT-2M tokamak, in *Plasma Physcis and Controlled Nuclear Fusion Research 1996,* (Proc. of the 16$^{\text{th}}$ Int. Conf., Montreal, 1996), Vol. 1, pages 167–175, Vienna, 1997, IAEA.

[6]M. Greenwald, R. L. Boivin, F. Bombarda, et al., *Nucl. Fusion*, **37**, 793 (1997).

[7]M. Greenwald, R. L. Boivin, P. Bonoli, et al., *Phys. Plasmas*, **6**, 1943 (1999).

[8]J. Terry, B. Lipschultz, A. Yu. Pigarov, et al., *Phys. Plasmas*, **5**, 1759 (1998).

[9]L. Johnson and E. Hinnov, *J. Quant. Spectrosc. Radiat. Transfer*, **13**, 333 (1973).

[10]R. Boivin, J. Goetz, E. Marmar, J. Rice, and J. Terry, *Rev. Sci. Instrum.*, **70**, 260 (1999).

[11]D. B. Heifetz, D. Post, M. Petravic, J. Weisheit, and G. Bateman, *J. Comput. Phys.*, **46**, 289 (1982).

[12]S. Tamor, *J. Comput. Phys.*, **40**, 104 (1981).

[13]V. Lebedev, P. Diamond, and B. Carreras, 1999, Bull. Am. Phys. Soc. 44, page 275.

[14]L. Owen, B. Carreras, P. Mioduszewski, R. Boivin, A. Hubbard, B. LaBombard, C. S. Pitcher, and J. Terry, 1998, Bull. Am. Phys. Soc. 43, page 1823.

[15]P. Mioduszewski, B. Carreras, L. Owen, R. Boivin, A. Hubbard, B. LaBombard, J. Terry and M. Umansky, 1999, Bull. Am. Phys. Soc. 44, page 208.

[16]M. Umansky, S. Krasheninnikov, B. LaBombard, and J. Terry, *Phys. Plasmas*, **5**, 3373 (1998).

[17]M. V. Umansky, S. Krasheninnikov, B. LaBombard, B. Lipschultz, and J. Terry, *Phys. Plasmas*, **6**, 2791 (1999).

[18]C. S. Pitcher, C. J. Boswell, J. A. Goetz, B. LaBombard, B. Lipschultz, J. E. Rice and J. L. Terry, 1999, Bull. Am. Phys. Soc. 44, page 287.

[19]V. Lebedev, P. Diamond, and B. Carreras, 1999, Bull. Am. Phys. Soc. 44, page 275.

[20]A. Hubbard, R. L. Boivin, R. S. Granetz, et al., *Phys. Plasmas*, **5**, 1744 (1998).

[21]W. Rowan, A. G. Meigs, E. R. Solano, P. M. Velanju, M. D. Calvin, and R. D. Hazeltine, *Phys. Fluids B***5**, 2485 (1993).

[22]T. Fülöp, P. Catto, and P. Helander, *Phys. Plasmas*, **5**, 3969 (1998).

[23]S. Krasheninnikov, P. J. Catto, D. J. Sigmar, et al., Tokamak Divertor and Stability, and Atomic Physics and ExB Drift Modifications of Strongly Inhomogeneous Edge Plasmas, in *Plasma Physics and Controlled Nuclear Fusion Research 1998,* (Proc. of the 17$^{\text{th}}$ Int. Conf., Yokohama, 1998), Vol. 1, Vienna, 1998, IAEA, IAEA-F1-CN-69/TH3/6.

[24]P. Catto, P. Helander, J. Connor, and R. Hazeltine, *Phys. Plasmas*, **5**, 3961 (1998).

[25]I.H. Hutchinson, R. Granetz, A. Hubbard, J.A. Snipes, T. Sunn Pedersen, M. Greenwald, B. LaBombard, and the Alcator Group, *Plasma Phys. Control. Fusion*, **41**, A609 (1999).

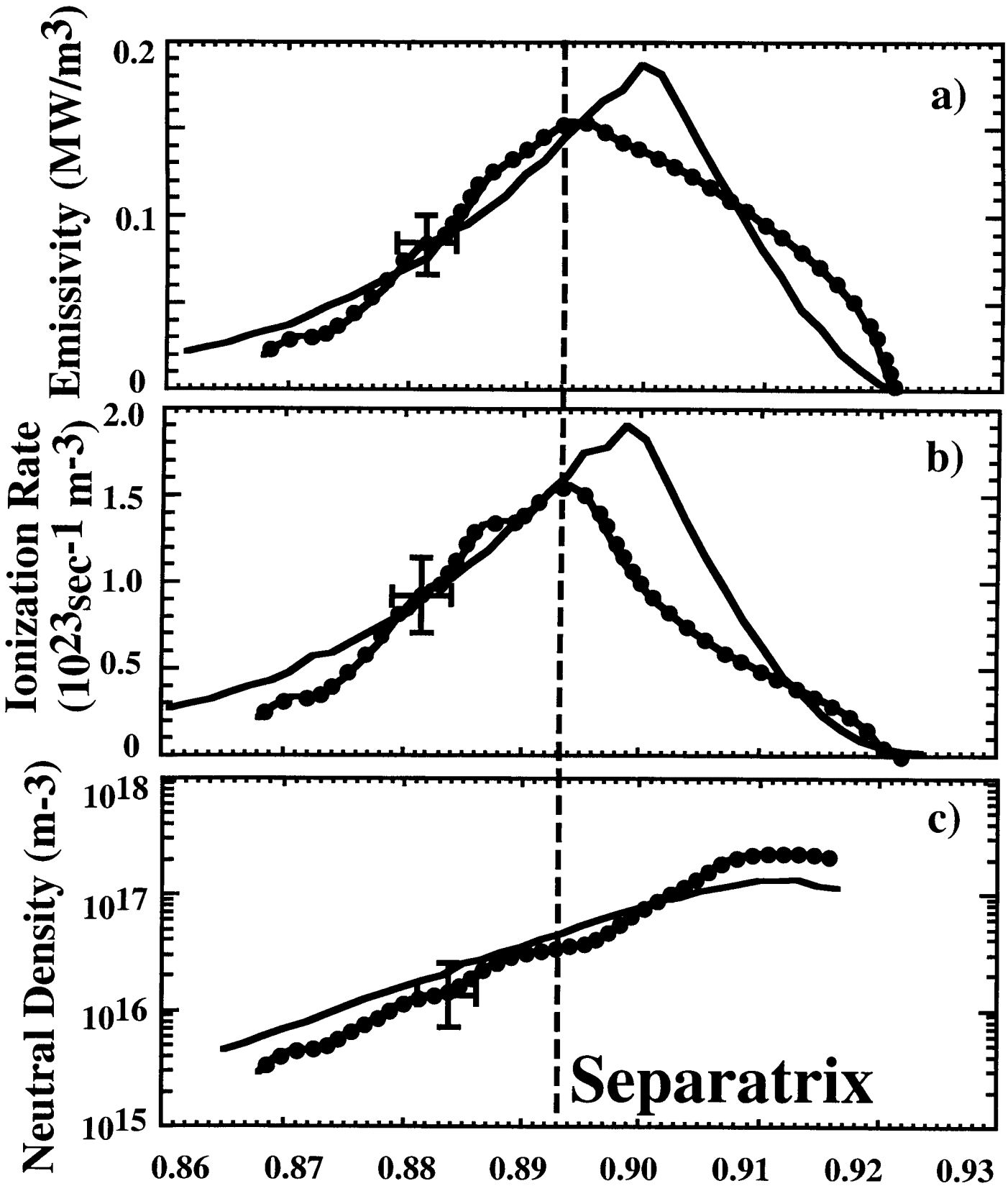
Emissivity (MW/m3)
0.2
0.1
0
a)
Ionization Rate (1023sec-1 m-3)
2.0
1.5
1.0
0.5
0
b)
Neutral Density (m-3)
10^18
10^17
10^16
10^15
c)
Separatrix
0.86
0.87
0.88
0.89
0.90
0.91
0.92
0.93
Major Radius (m)

Figure 1a

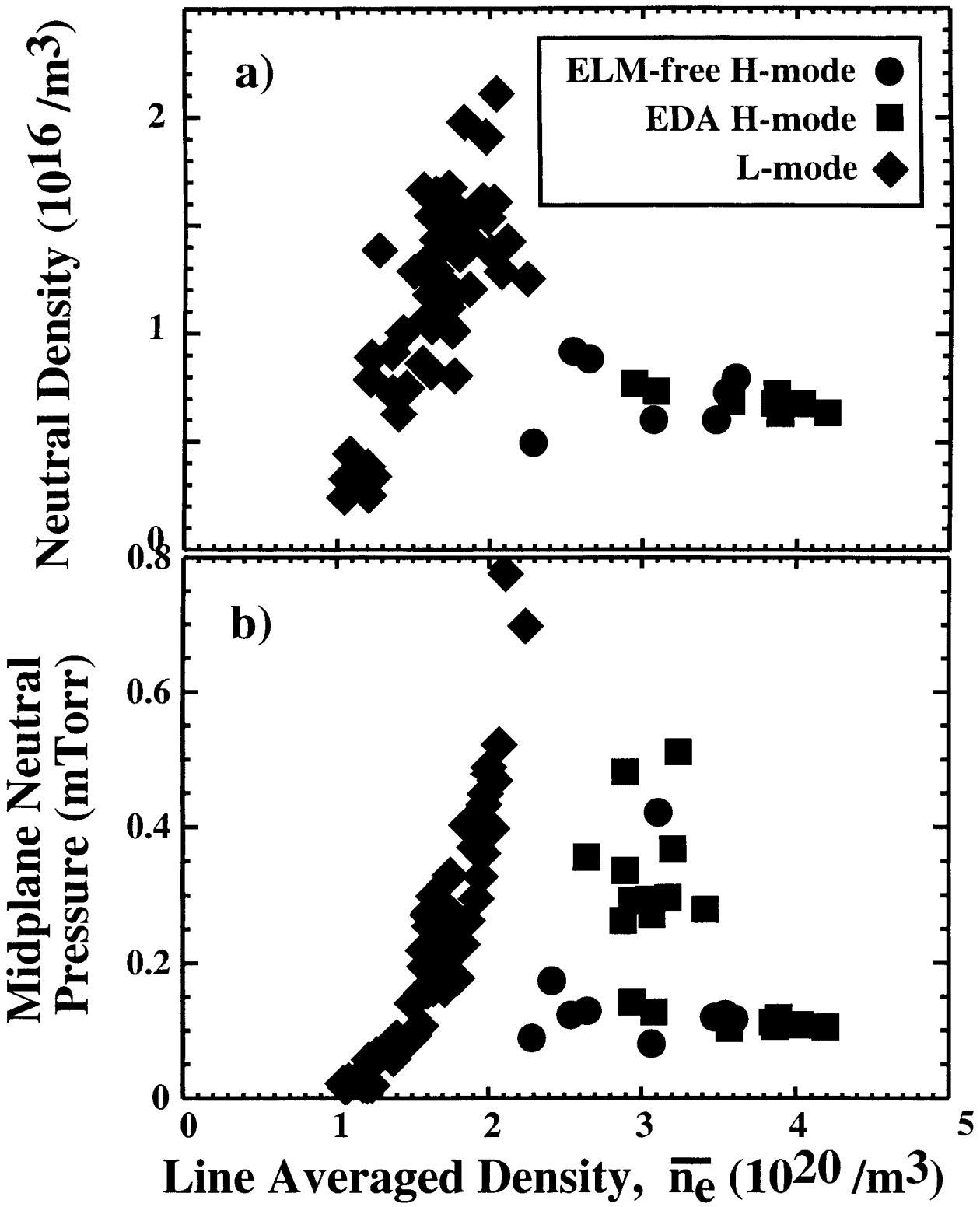
a)
ELM-free H-mode
EDA H-mode
L-mode
Neutral Density (10^{16} /m^3)
0
1
2
b)
Midplane Neutral Pressure (mTorr)
0
0.2
0.4
0.6
0.8
0
1
2
3
4
5
Line Averaged Density, $\overline{n_e}$ (10^{20} /m^3)

Figure 1b

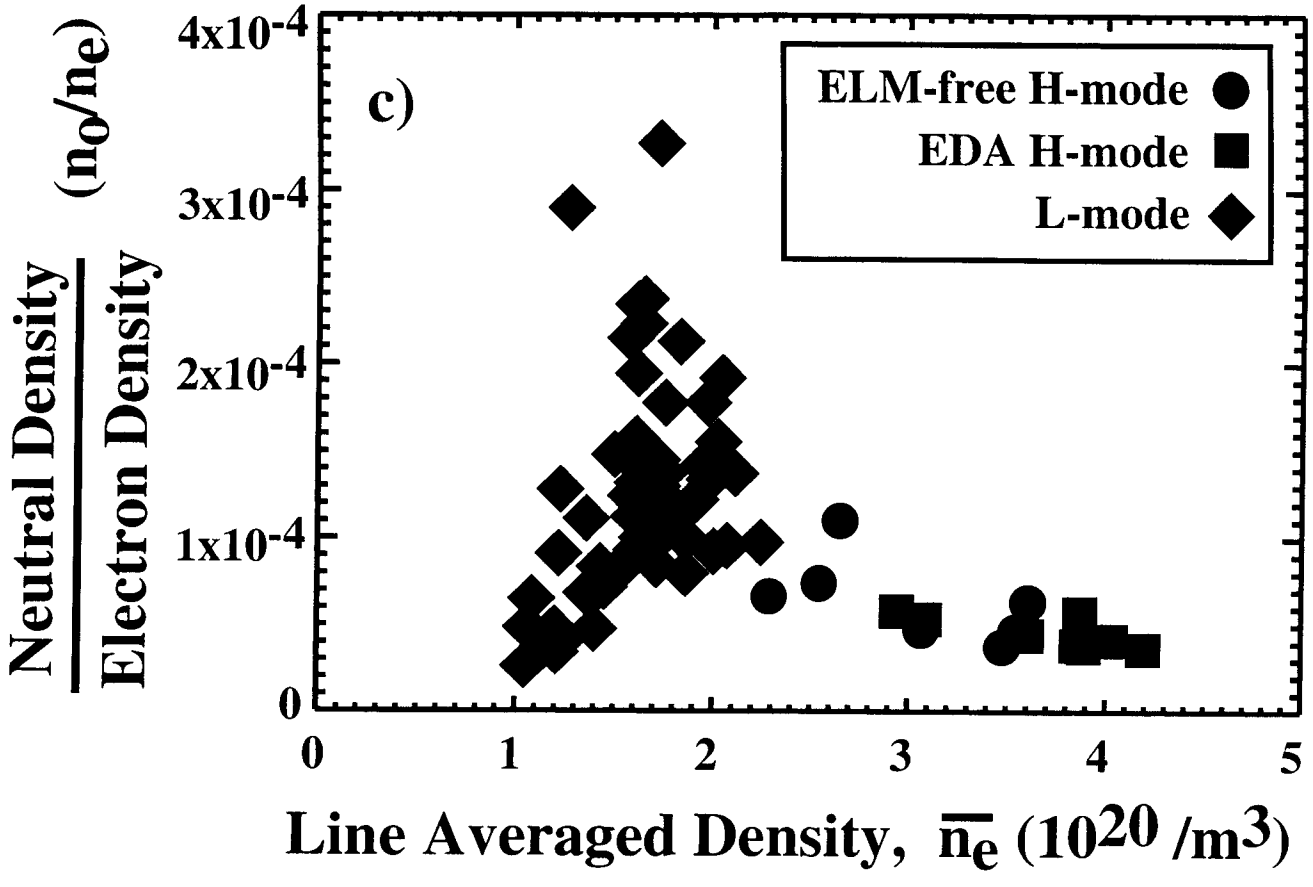
c)
ELM-free H-mode
EDA H-mode
L-mode
Neutral Density / Electron Density (n_0/n_e)
4x10-4
3x10-4
2x10-4
1x10-4
0
0
1
2
3
4
5
Line Averaged Density, $\overline{n_e}$ (10^{20} /m3)

Figure 1c

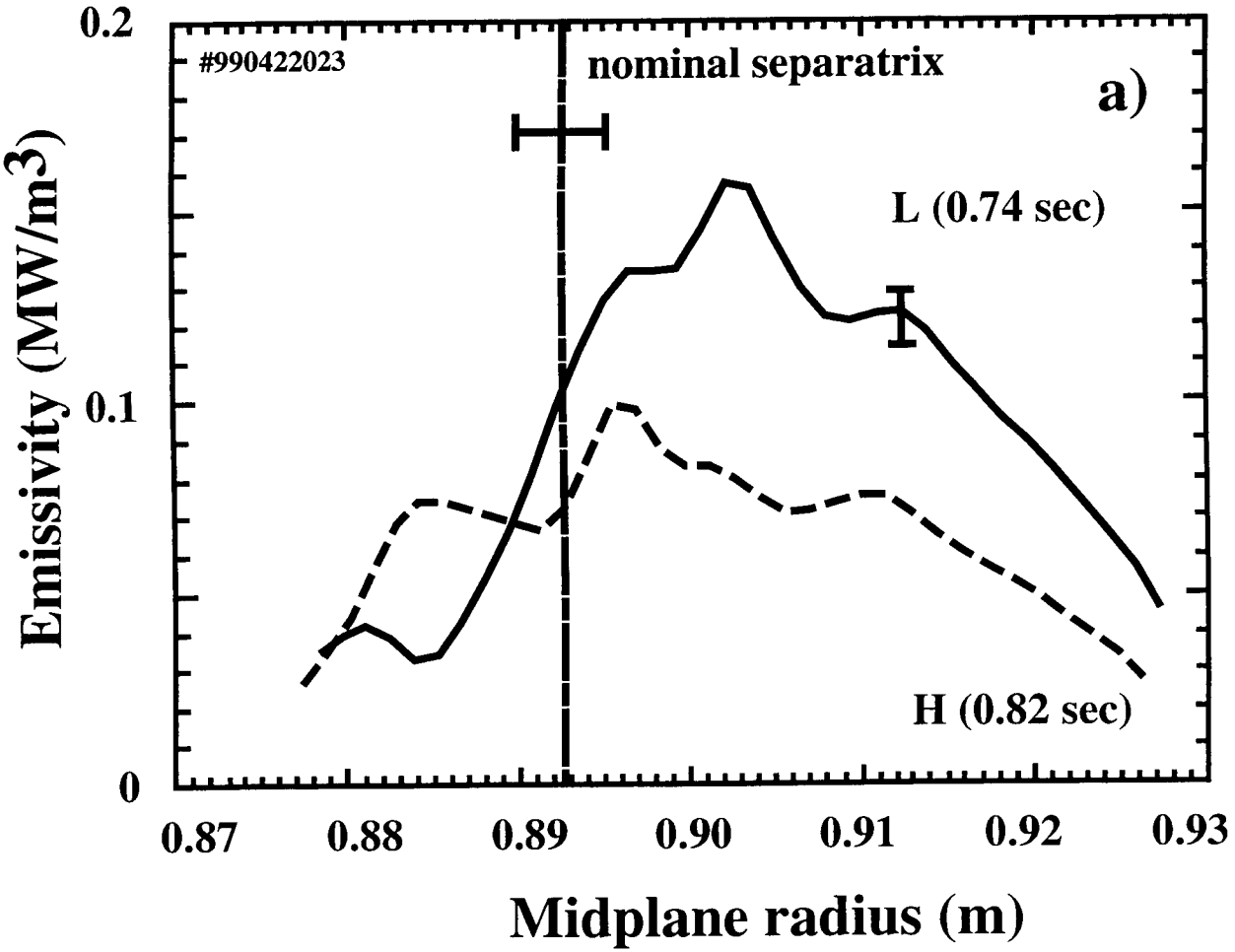
#990422023
nominal separatrix
a)
L (0.74 sec)
H (0.82 sec)
Emissivity (MW/m3)
0.2
0.1
0
0.87
0.88
0.89
0.90
0.91
0.92
0.93
Midplane radius (m)

Figure 2a

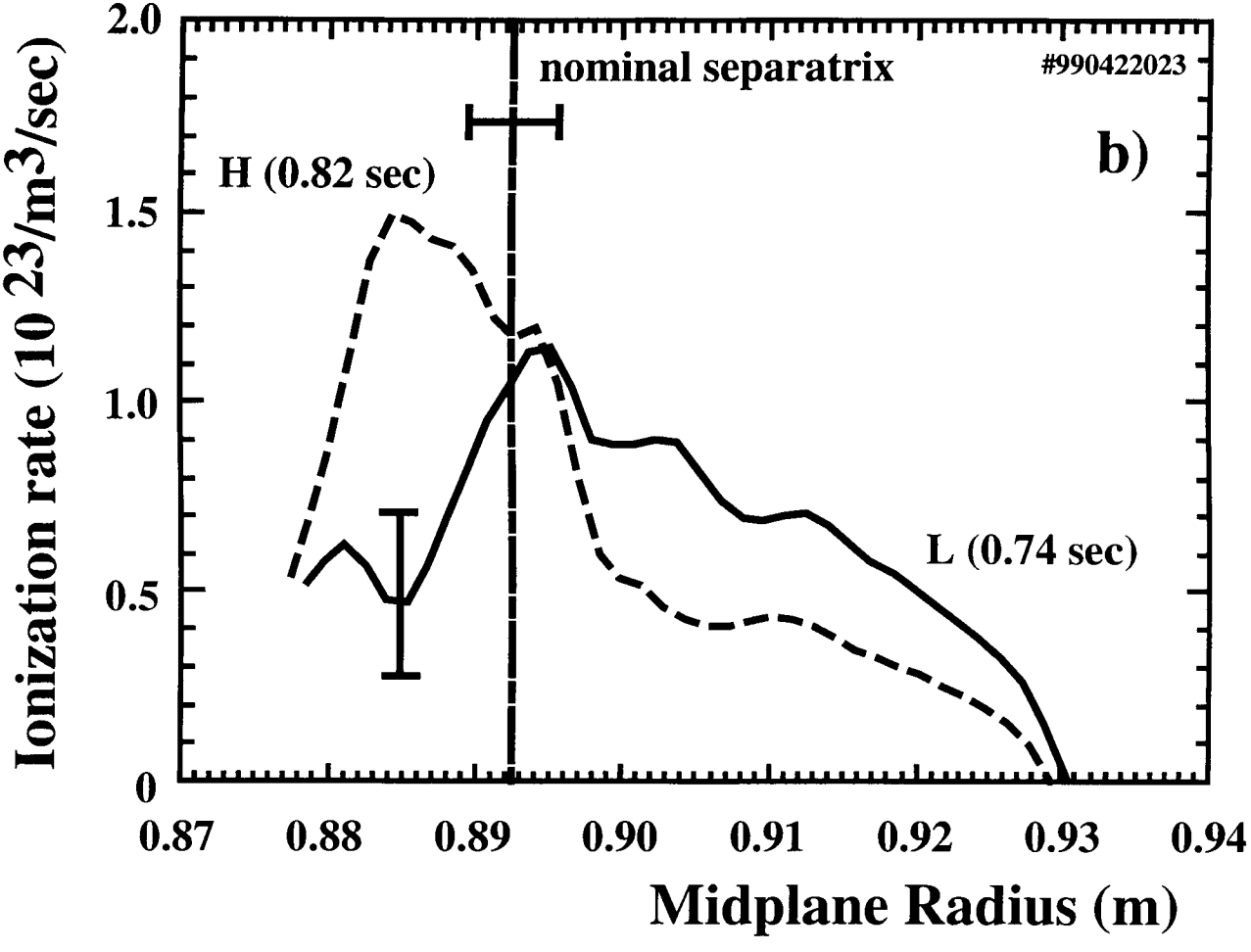
2.0
1.5
1.0
0.5
0
Ionization rate (10 23/m3/sec)
nominal separatrix
#990422023
b)
H (0.82 sec)
L (0.74 sec)
0.87
0.88
0.89
0.90
0.91
0.92
0.93
0.94
Midplane Radius (m)

Figure 2b

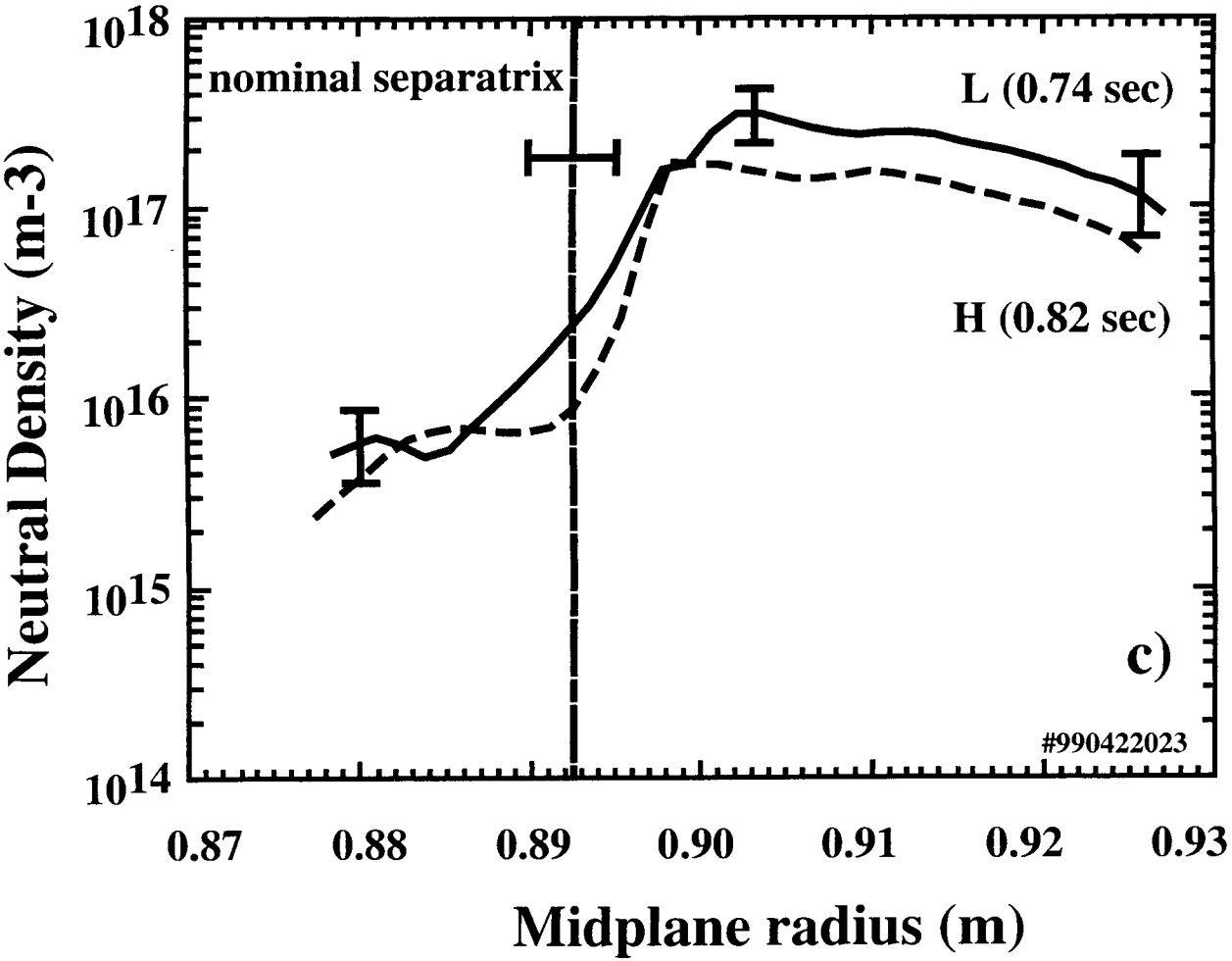
nominal separatrix
L (0.74 sec)
H (0.82 sec)
c)
#990422023
Neutral Density (m-3)
10^{18}
10^{17}
10^{16}
10^{15}
10^{14}
0.87
0.88
0.89
0.90
0.91
0.92
0.93
Midplane radius (m)

Figure 2c

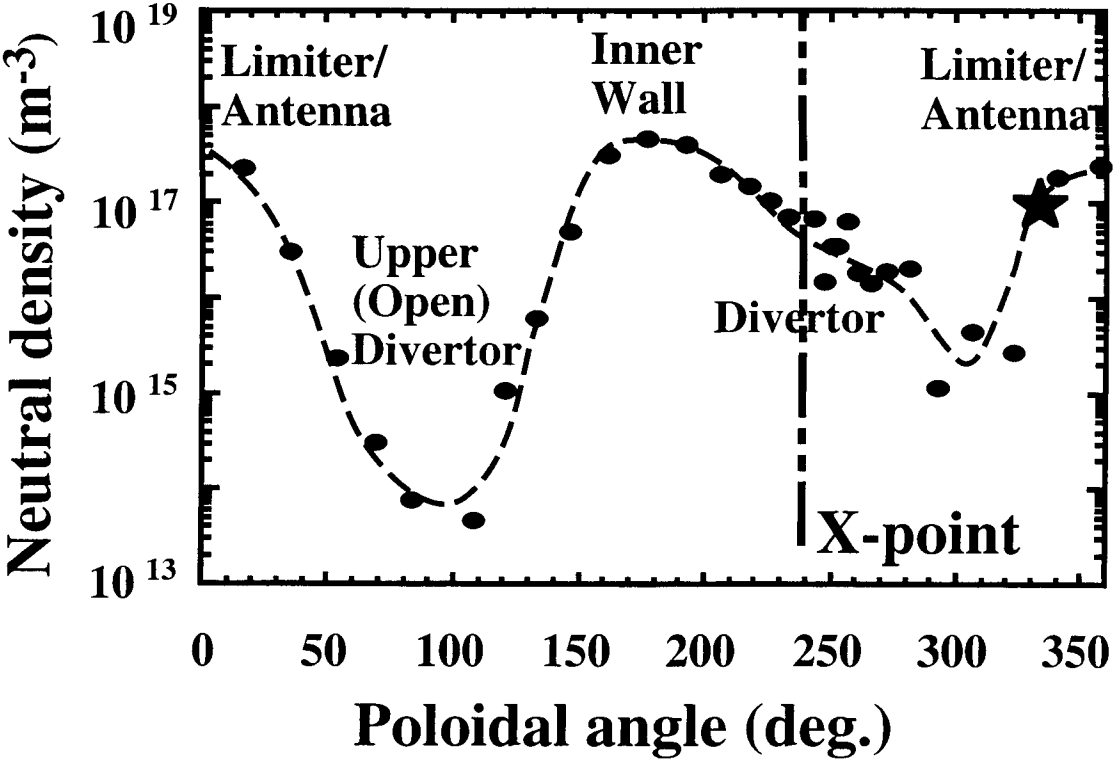
Neutral density (m-3)
10 19
10 17
10 15
10 13
Limiter/
Antenna
Inner
Wall
Limiter/
Antenna
Upper
(Open)
Divertor
Divertor
X-point
0
50
100
150
200
250
300
350
Poloidal angle (deg.)

Figure 3a

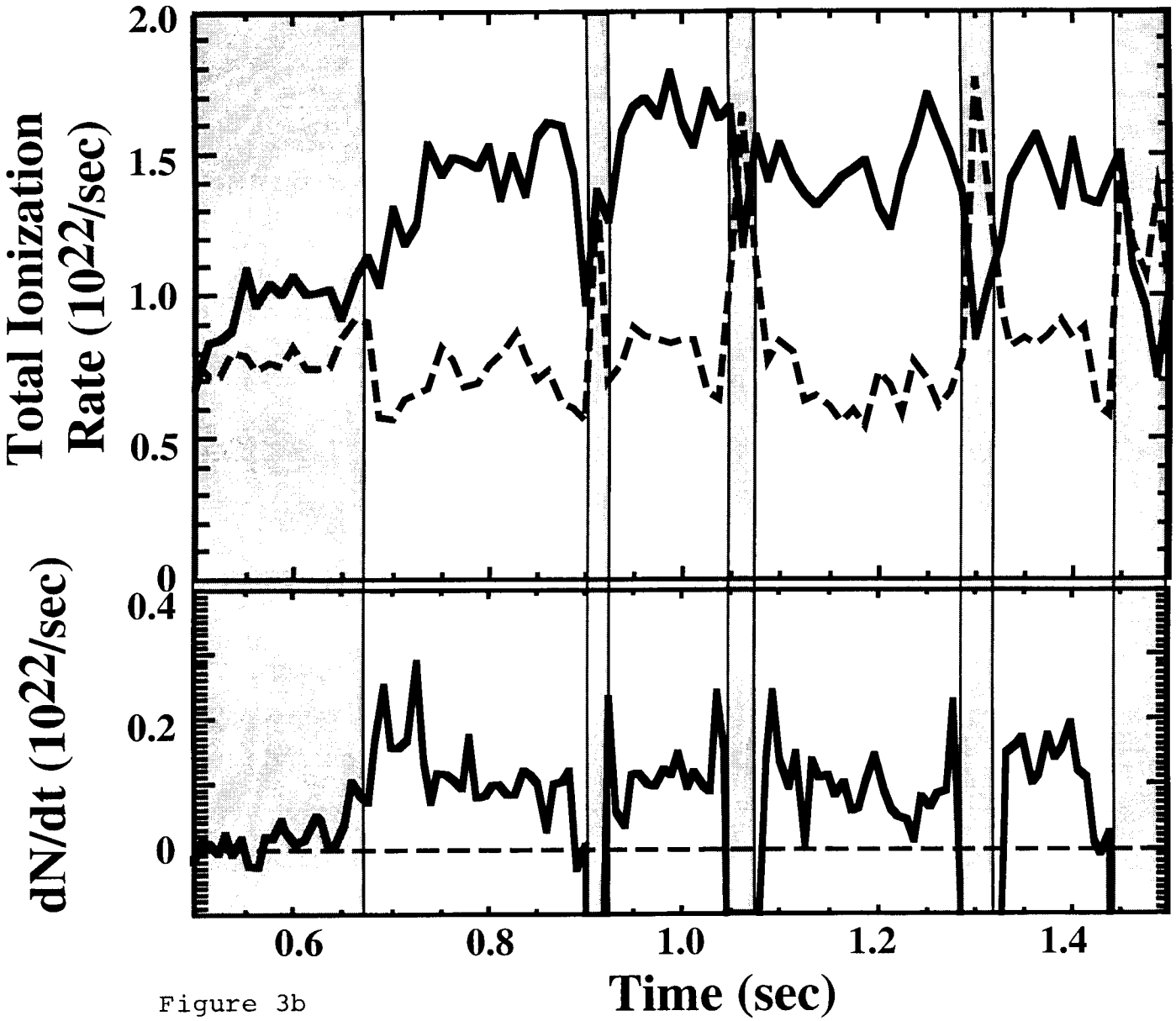
Total Ionization Rate (1022/sec)
2.0
1.5
1.0
0.5
0
dN/dt (1022/sec)
0.4
0.2
0
0.6
0.8
1.0
1.2
1.4
Time (sec)

Figure 3b

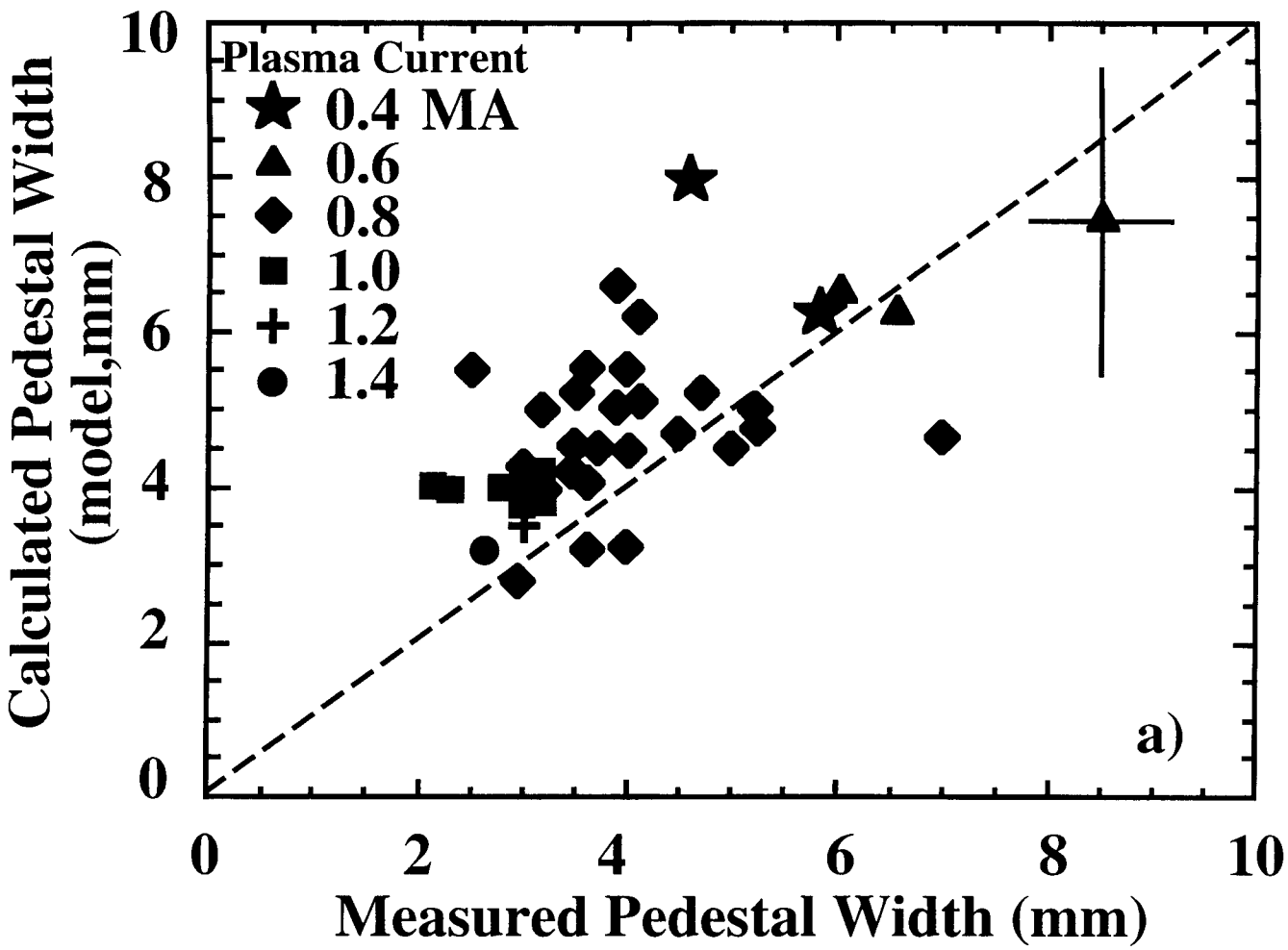
Plasma Current
0.4 MA
0.6
0.8
1.0
1.2
1.4
a)
Calculated Pedestal Width (model,mm)
Measured Pedestal Width (mm)
0
2
4
6
8
10

Figure 3c

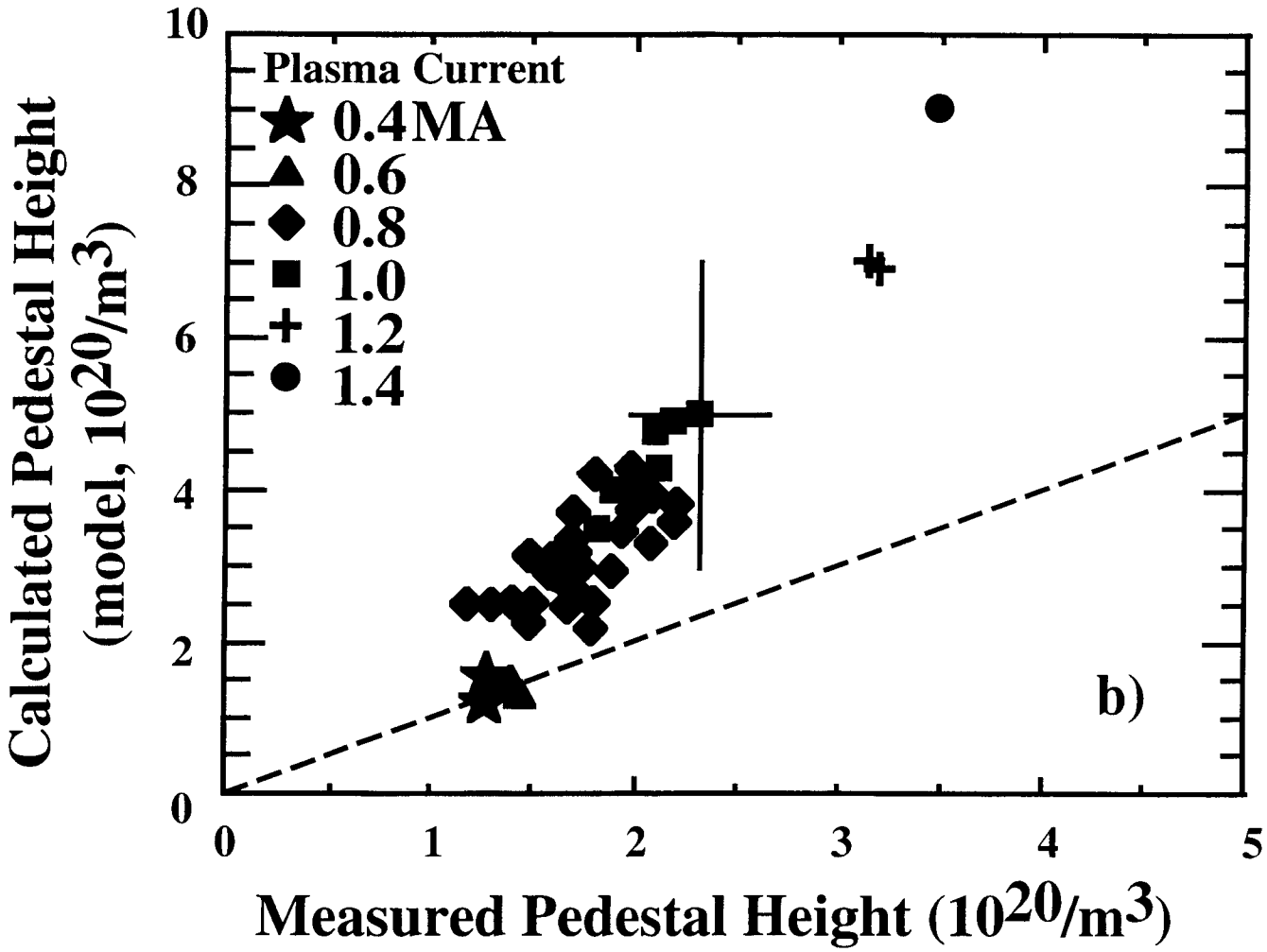
Plasma Current
0.4MA
0.6
0.8
1.0
1.2
1.4
b)
Calculated Pedestal Height (model, $10^{20}/m^3$)
Measured Pedestal Height ($10^{20}/m^3$)
0
1
2
3
4
5
0
2
4
6
8
10

Figure 4

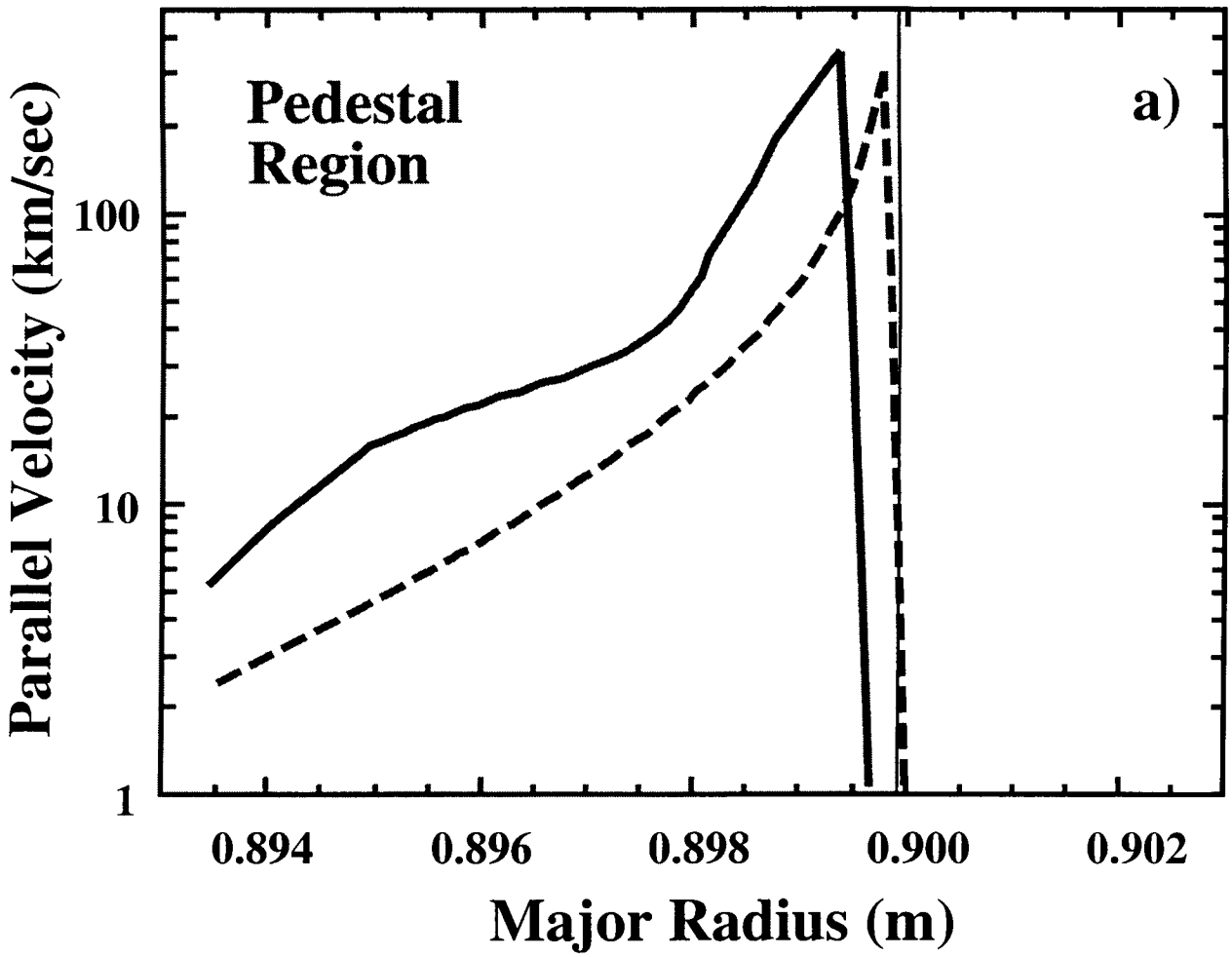
Pedestal
Region
a)
Parallel Velocity (km/sec)
100
10
1
0.894
0.896
0.898
0.900
0.902
Major Radius (m)

Figure 5

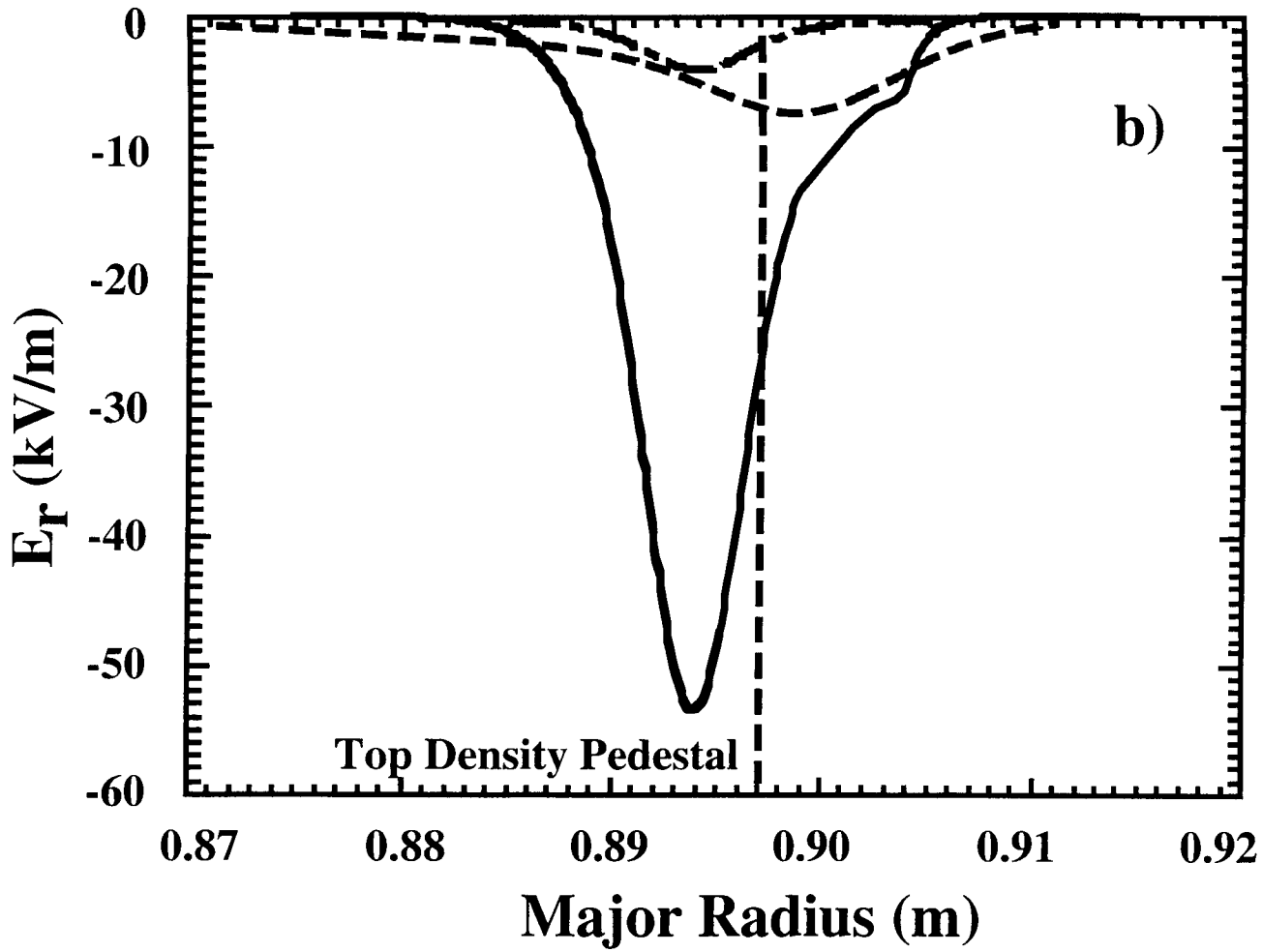
0
-10
-20
-30
-40
-50
-60
E_r (kV/m)
b)
Top Density Pedestal
0.87
0.88
0.89
0.90
0.91
0.92
Major Radius (m)

Figure 6a

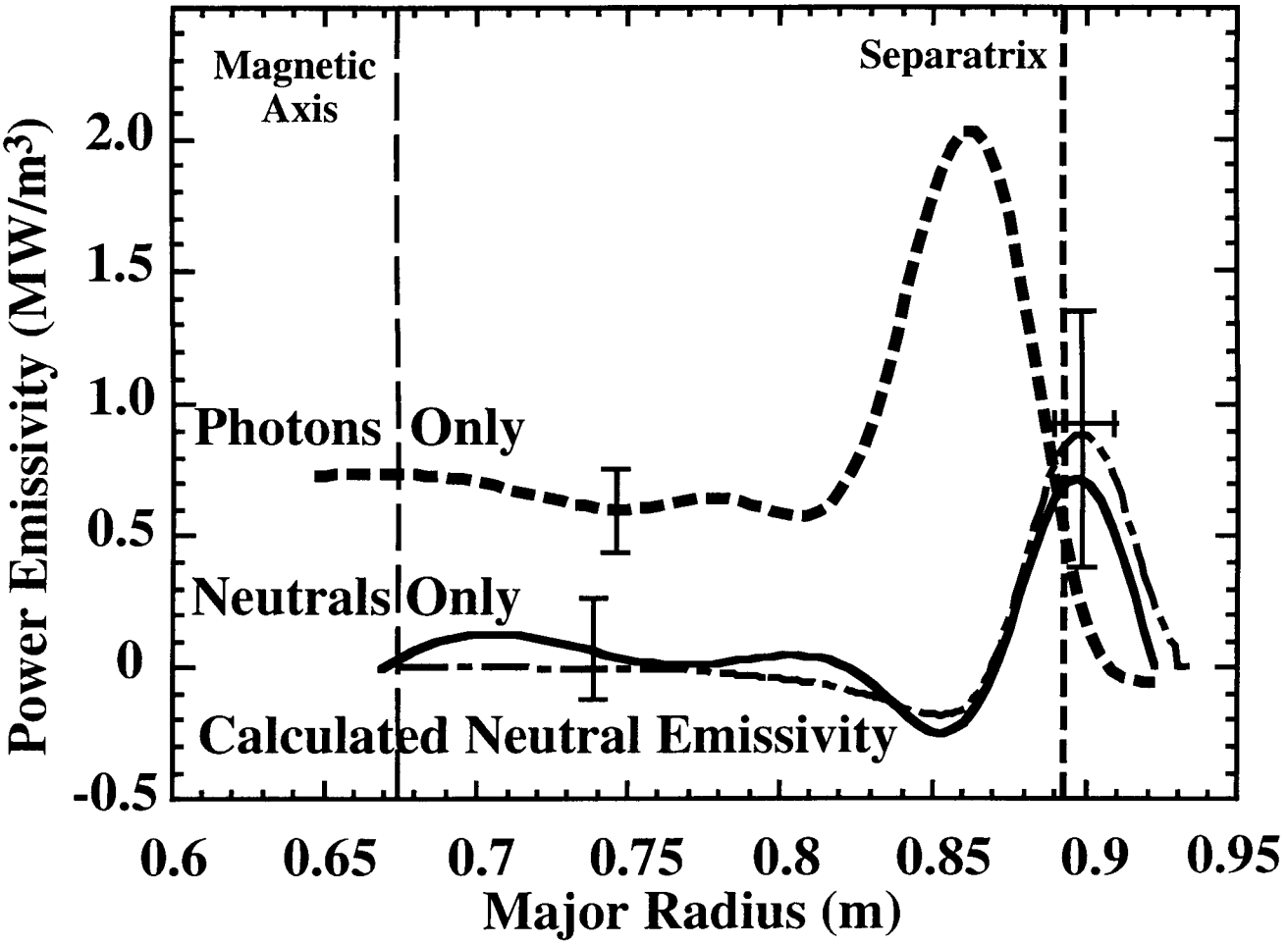
Magnetic Axis
Separatrix
Photons Only
Neutrals Only
Calculated Neutral Emissivity
Power Emissivity (MW/m³)
2.0
1.5
1.0
0.5
0
-0.5
0.6
0.65
0.7
0.75
0.8
0.85
0.9
0.95
Major Radius (m)

Figure 6b